Immunophysical Properties and Prediction of Activities for Vaccinia Virus Complement Control Protein and Smallpox Inhibitor of Complement Enzymes Using Molecular Dynamics and Electrostatics

Li Zhang* and Dimitrios Morikis†
*Department of Chemistry, and †Department of Chemical and Environmental Engineering, University of California, Riverside, California 92521

ABSTRACT We present immunophysical modeling for VCP, SPICE, and three mutants using MD simulations and Poisson-Boltzmann-type electrostatic calculations. VCP and SPICE are homologous viral proteins that control the complement system by imitating, structurally and functionally, natural regulators of complement activation. VCP and SPICE consist of four CCP modules connected with short flexible loops. MD simulations demonstrate that the rather complex modules of VCP/SPICE and their mutants exhibit a high degree of intermodular spatial mobility, which is affected by surface mutations. Electrostatic calculations using snapshots from the MD trajectories demonstrate variable spatial distribution of the electrostatic potentials, which suggests dynamic binding properties. We use covariance analysis to identify correlated modular oscillations. We also use electrostatic similarity indices to cluster proteins with common electrostatic properties. Our results are compared with experimental data to form correlations between the overall positive electrostatic potential of VCP/SPICE with binding and activity. We show how these correlations can be used to predict binding and activity properties. This work is expected to be useful for understanding the function of native CCP-containing regulators of complement activation and receptors and for the design of antiviral therapeutics and complement inhibitors.

INTRODUCTION

The complement system is an evolutionarily ancient form of innate immunity and a bridge between innate and adaptive immunities (1–5). The complement system has mechanisms in place for recognition, binding, and elimination of foreign pathogens, among them viruses and virally infected cells. On the other hand, viruses have evolved mechanisms for evasion of the complement system and immune system in general (6–8). The variola and vaccinia viruses, both members of the genus *Orthopoxvirus*, are capable of inhibiting and regulating the complement system by mimicking the function of natural RCAs (9–12). The variola virus is the causative agent of smallpox disease, which was eradicated using the less potent vaccinia virus as an inoculation agent (11). Little is known of the mechanisms of function of the orthopoxviruses, and a renewed need to understand and inhibit their function has been generated with recent biosafety concerns (13,14).

The vaccinia virus encodes the VCP and the variola virus encodes the SPICE protein, which are secreted by infected cells (9–12). VCP and SPICE inhibit the activation of the complement system by acting on complement components C3b and C4b and disallowing their function. VCP acts as a cofactor of Factor I in the enzymatic cleavage and inactivation of C3b and C4b and accelerates the decay of C3 convertase complexes (which contain C3b or C4b) (6–12). SPICE is also known to act as a cofactor of Factor I in the enzymatic cleavage and inactivation of C3b and C4b (10,11). C3b and C4b are the opsonins that coat the surfaces of infecting viruses for recognition and elimination by phagocytes. C3b and C4b are also building blocks of the so-called C3 and C5 convertase enzymes, which are responsible for the cleavage of C3 to C3a and C3b and C5 to C5a and C5b. C3a and C5a are promoters of inflammatory response and C5b is a building block of MAC, which is capable of lysing the membranes of cell-free viruses. The complement system is finely regulated by RCAs, such as C4BP, CR1, MCP, DAF, and Factor H, and interacts with CRs such as CR1 (also an RCA) and CR2 (not an RCA). The regulated complement components by RCAs are C3b and C4b and their variants and the convertases they form. A structural overview of the complement activation and regulation pathways, CRs, and selected inhibitors has been presented (15). Also, a structural classification of RCAs has been presented (16).

VCP, SPICE, most RCAs, and CRs have similar sequence and structural characteristics. They are modular proteins containing several CCP modules, also known as SCR

Submitted June 7, 2005, and accepted for publication January 18, 2006.

Address reprint requests to Dimitrios Morikis, Dept. of Chemical and Environmental Engineering, University of California, Riverside, CA 92521. Tel.: 951-827-2696; E-mail: dmorikis@engr.ucr.edu.

Abbreviations used: VCP, vaccinia virus complement control protein; SPICE, smallpox inhibitor of complement enzymes; RCA, regulator of complement activation; CCP, complement control protein; SCR, short consensus repeat; CR, complement receptor; CR1, complement receptor 1; CR2 complement receptor 2; C3, complement component C3; MCP, membrane cofactor protein; DAF, decay accelerating factor; PDB, Protein Data Bank; MD, molecular dynamics; RMSD, root mean-square deviation; SASA, solvent accessible surface area; ESI, electrostatic similarity index; MAC, membrane attack complex; C4BP, C4-binding protein; EEF1, effective energy function 1; ABNR, adopted-basis Newton-Raphson; NOE, nuclear Overhauser effect; KCP, Kaposi's sarcoma-associated herpesvirus complement control protein; NVT, constant number of particles, volume, and temperature statistical ensemble; OXT, second oxygen atom of the C-terminus carboxyl group.

0006-3495/06/05/3106/14 $2.00 doi: 10.1529/biophysj.105.068130

modules, connected by flexible loops to form long chains (16). VCP and SPICE are formed by four CCP modules, which are arranged in a nearly linear chain according to the x-ray diffraction structures of the four-module protein (17,18) or the NMR structures of two-module fragments (19,20). The structural resemblance of VCP and SPICE to RCAs is responsible for the complement system evasion by their respected vaccinia and variola viruses. The mechanism of binding of VCP and SPICE to their targets, C3b and C4b, and resulting inhibition of complement activation is largely unknown. This makes necessary structural and computational studies at atomic level to understand the physicochemical properties of VCP/SPICE responsible for binding and inhibition.

VCP and SPICE differ by only 11 amino acids, but their inhibitory activities differ by up to 1000-fold, with SPICE being more active. A recent study has shown that SPICE is 75-fold and 1000-fold more active than VCP in inhibiting the classical and the alternative pathways, respectively, of complement activation (21). An earlier study had shown that SPICE was 100-fold and 6-fold more potent than VCP in inactivating C3b and C4b, respectively, in the presence of Factor I (22). There are subtleties in the activities of VCP and SPICE. VCP is a better inhibitor of the classical pathway, whereas SPICE is a better inhibitor of the alternative pathway of complement activation (21). Both VCP and SPICE exhibit species specificity (22). The study by Sfyroera et al. (21) has pointed out the importance of the modulation of the electrostatic potential of VCP, SPICE, and several mutants in the binding to C3b and in inhibiting complement activation by using a static crystallographic structure of VCP and a modeled structure of SPICE. Here, we present immunophysical modeling of VCP and SPICE. We have performed a detailed analysis of the physicochemical properties of VCP and SPICE that are responsible in modulating their electrostatic potentials, including their dynamics.

Our modeling involves MD simulations and electrostatic calculations. We have used MD to explore the conformational space of VCP and SPICE. We have examined the flexibility, mobility, and correlated motions of the four modules of VCP and SPICE by analyzing the MD trajectories. Furthermore, we have explored the ionization properties and the spatial distribution of charge and electrostatic potentials using the MD data and electrostatic calculations based on the solution of the Poisson-Boltzmann equation. We use our data to explain the differences in the activities of the two proteins. In addition, we use our data to predict the minimum number of mutations that are sufficient to increase or reduce the activities of VCP and SPICE. Most of our results are compared to experimental mutagenesis, binding, and activity data. We discuss our proposed binding model in view of earlier studies involving the interaction of C3d with CR2 (23) because of a similar predominant role of electrostatics in binding. Also, we discuss similarities between the structural and functional characteristics of VCP/SPICE with CR1, MCP, and DAF because VCP has CR1-, MCP-, and DAF-like activities (6).

This work contributes to our current understanding of the function of VCP and SPICE by providing mechanistic modeling at atomic and biomolecular levels. We expect that our models and predictions will be useful in the renewed interest in the design of antiviral therapeutics (14). We also expect that this work will contribute to our understanding of the function of regulators of complement activation and receptors, for which CCPs are the basic building blocks. This knowledge will aid in the design of complement inhibitors useful against several pathological situations where unregulated complement activation is observed. Methodologically, this work shows the power of computational physical methods for immunology research (24).

METHODS

Structural modeling

Our computational modeling is based on the crystallographic structure of VCP with PDB (25) Code 1G40 (17). Chain A of 1G40 was extracted from the dimeric VCP crystal structure and was used for structural homology modeling of SPICE, VCP2m, VCP3m, and VCP4m. We used the program Swiss PDB Viewer (26) to incorporate mutations in the structure 1G40 of VCP. Energy minimization was performed to optimize the conformation of the mutating amino acids. The sequences of the modeled structures are given in Fig. 1. There are 2–11 mutations in the modeled structures compared to VCP, 2 in VCP2m, 3 in VCP3m, 4 in VCP4m, and 11 in SPICE. The crystal structure of VCP and the modeled structures of SPICE, VCP2m, VCP3m, and VCP4m were used in the MD simulations (see below).

MD simulations

The program CHARMM (27) version 31b1 was used to perform MD simulations with the EEF1 implicit solvent model (28). EEF1 adds solvation-free energy to the vacuum-free energy function of a biomolecule. The solvation-free energy contains contributions from two effects, the exclusion of solvent from the space occupied by solute groups (self-energy of charges) and modifications of the solvent in the nonsolute remaining space (dielectric screening of interactions between all pairs of solute charges). The authors of EEF1 point out that this solvation model is useful to discriminate native conformations from misfolded decoys (29,30). In this work, values of all the parameters of the EEF1 model were set to their default values as implemented in the CHARMM 31b1 program with an electrostatic and van der Waals cutoff of 9 Å and a switching function between 7 and 9 Å. EEF1 uses the CHARMM 19 polar hydrogen energy function. The SHAKE algorithm (31) was used to fix the length of covalent bonds of hydrogen atoms. The time step was set to 1 fs. We have enforced disulfide bridges as shown in Fig. 1, using patches in CHARMM. All structures were first energy minimized for 300 steps with the ABNR method. Then, the systems were subjected to 5 ps of constant volume MD simulation, during which the temperature of the system was raised from 0 K to 300 K with velocity rescaled every 0.1 ps. At 300 K, 30 ps equilibration phase was initiated, with velocity rescaled every 0.1 ps during the first 10 ps. In the later stage of the equilibration, velocity was rescaled only if the temperature of the system deviated more than 5 K from 300 K. At the end of the equilibration, energy and temperature were stable, and no velocity rescaling was necessary for the last 10 ps. After the equilibration, 10 ns of NVT MD at 300 K was run with a Nose-Hoover thermostat (32,33). Coordinate sets were sampled every 10 ps to generate 1000 snapshots of structures during the MD trajectory. Energy minimization was performed at the end of each MD snapshot.

CHARMM utilities and homemade programs were used to analyze the MD trajectories. The RMSD time series, averaged over the N, C_α, and C

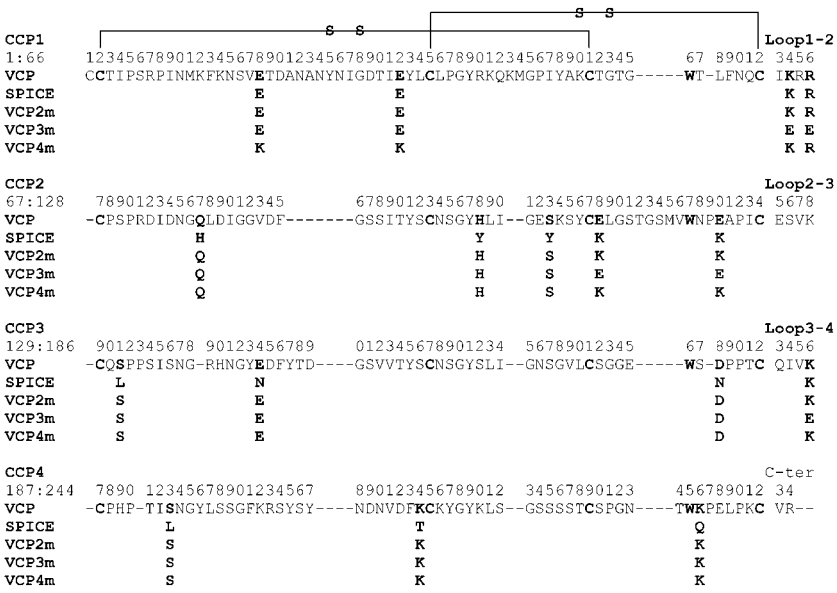

FIGURE 1 Sequence alignment of VCP, SPICE, VCP2m, VCP3m, and VCP4m. Only mutated amino acids are shown for SPICE, VCP2m, VCP3m, and VCP4m, the remaining amino acids being the same as in VCP. The figure also displays the alignment of the four CCP modules with respect to each other. In each CCP module, there are four conserved cysteines forming two disulfide bridges (marked in figure) and a single conserved tryptophan. The end amino acids of each CCP module are the first and fourth of the conserved cysteines.

backbone heavy atoms, were calculated relative to the minimized crystal structure. The relative intermodular position of two CCP domains was characterized by tilt, twist, and skew angles (16,19,20,34–37). The boundaries of each single CCP domain were defined by the first and fourth disulfide-bonded cysteines (Fig. 1). To define the coordinate system of each domain, we set the center of its mass as the origin point of the domain, and the z axis was aligned with the principal inertia tensor of the domain pointing toward the C-terminus. The direction of the x axis was defined with reference to C_α atom of the consensus conserved Trp (see Fig. 1 for Trp location). The y axis was determined by the right-hand rule. To calculate the angles between the neighboring domains, centers of masses of the neighboring domains were superimposed without changing any of the angles. A homemade FORTRAN program was used to calculate the tilt, skew, and twist angles, using the mathematical formulas described in Lehtinen et al. (35). Note that we have calculated the principal inertia tensor using CHARMM with only polar hydrogen atoms present. Also, the first (free) cysteine, the intermodular loops, and the two-amino acid C-terminal loop (Fig. 1) are not considered in our calculation of principal inertia tensors. These selections may be different from other calculations in the literature (16,20,34–36). SASA was calculated using CHARMM with a probe radius 1.4 Å. The differences in SASA (ΔSASA) were calculated according to $\Delta\text{SASA} = \Sigma_i[\text{SASA}(\text{CCP}_i)] - \text{SASA}[\Sigma_i(\text{CCP}_i)]$, where i refers to module number. In the SASA calculations the length of individual CCP modules is defined in the rows of Fig. 1, including loops outside the disulfide bonded cysteines.

Covariance analysis of the intermodular mobility was performed using the 10-ns MD trajectories of VCP, SPICE, VCP2m, VCP3m, and VCP4m. Equal-time covariances were calculated for the displacement vectors Δr_i and Δr_j of modules i and j according to $c(i,j) = \langle \Delta r_i \cdot \Delta r_j \rangle$, where the brackets denote ensemble average (38). The displacement vectors were defined from the protein center of mass to the center of mass of each CCP module. The center of mass was calculated using C_α-atoms, and the constituent amino acids of each CCP module are shown in Fig. 1. The ensemble average is estimated from the MD trajectory according to $c(i,j) = (1/N)\sum_{n=1}^{N} \Delta r_i(t_n)\Delta r_j(t_n)$, where $\Delta r_i(t_n)$ is the displacement of module i at time t_n with respect to its average position during the trajectory and $N = 1000$ is our number of MD snapshots. The cross correlation between modules i and j were calculated according to $C(i,j) = (c(i,j))/(\sqrt{c(i,i)c(j,j)}) = (\langle \Delta r_i \cdot \Delta r_j \rangle)/(\sqrt{\langle \Delta r_i^2 \rangle \langle \Delta r_j^2 \rangle})$, where $C(i,j) = 1$ for completely correlated motions, $C(i,j) = -1$ for completely anticorrelated motions, and $C(i,j) = 0$ for uncorrelated motions. The quantity $C(i,j)$ describes correlated modular oscillations when the angles formed by the motional directions of the two modules are close to 0° or 180°. In other words, $C(i,j)$ depicts if the two modules move together in the same direction or in opposite directions but not more complex twist or orthogonal motions (39).

Electrostatic calculations

The calculation of apparent pK_a values of ionizable sites in the interior of proteins is possible if model and intrinsic pK_a values and the matrix of ionizable site-site interactions of all ionizable sites are available. The model pK_a is an experimental quantity that corresponds to the ionization of a free ionizable site (amino acid) in solution. The intrinsic pK_a is a hypothetical quantity that corresponds to the pK_a of a specific ionizable site in the interior of the proteins in the absence of interaction with other ionizable sites, which are considered neutral. The apparent pK_a corresponds to the interaction of an ionizable site with all other ionizable sites in their ionized state. The method of Antosiewicz et al. (40,41), implemented within the program UHBD (42), was used for the calculation of intrinsic pK_a values for the final (10 ns) minimized MD structures. Apparent pK_a values were calculated using the clustering method (43), implemented within the program HYBRID (43). The finite difference Poisson-Boltzmann solver of UHBD was used to calculate the electrostatic potential with continuum solvent representation. Dielectric coefficients of 78.4 and 20 were used for the solvent and protein interior, respectively. The temperature was set to 298 K and the ionic strength was set to 150 mM salt concentration. The parameter set of charges and van der Waals radii PARSE (44) was used. The solvent probe that defines the molecular surface had a radius of 1.4 Å. Dielectric smoothing at the protein-solvent interface (45,46) was used with an ion exclusion layer defined by a probe of 2.0 Å radius. Finite difference focusing methods (47,48) were used in the calculations, with focusing grids of 4.0, 2.5, 1.25, 0.5, and 0.25 Å. The ionic strength dependence of the electrostatic potentials is calculated in the Boltzmann part of the Poisson-Boltzmann equation in the form of a variable that is a function of the Debye length (49).

The addition of hydrogen atoms for the pK_a calculations was accomplished using the program WHAT IF version 99 (50,51). The program WHAT IF was also used to perform a global hydrogen-bonding network optimization, which corrected for the side-chain orientation of nonoptimal His, Asn, and Gln amino acids and established the initial hydrogen position at the $N_{\epsilon 2}$ or $N_{\delta 1}$ atom of His. Finally, WHAT IF was used to establish the neutral state of Asp, Glu, and C-terminus amino acids by adding a hydrogen atom at the $O_{\delta 2}$, $O_{\epsilon 2}$, and OXT atoms, respectively. Changes from the neutral to the charged state of ionizable amino acids were made by adding a

±1 charge to each ionizable site, depending on their charge. Positive unit charges were added at the backbone amide N atom of the N-terminus, N_ζ of Lys, and C_ζ of Arg amino acids. The WHAT IF hydrogen-bonding optimization calculation showed that the initial hydrogen atom in all His amino acids was located at the $N_{\delta 1}$ position, thus the +1 charge was added at $N_{\varepsilon 2}$. Negative unit charges were added at the backbone carboxyl C atom of the C-terminus, C_γ of Asp, C_δ of Glu, O_η of Tyr, and S_γ of free Cys amino acids. The experimental model pK_a values were 12.0 for Arg, 10.4 for Lys, 9.6 for Tyr, 8.3 for Cys, 6.3 for His, 4.4 for Glu, 4.0 for Asp, 7.5 for the N-terminus, and 3.8 for the C-terminus.

Electrostatic potential calculations for the isopotential contour plots were performed using the program GRASP (49,52), with the PARSE parameter set (44), dielectric coefficients of 4 and 78.5 for the protein and solvent, respectively, solvent radius of 1.4 Å, in the absence of salt, and in the presence of 150 mM salt. In the structures used for the GRASP calculations, hydrogens were added and optimized for their hydrogen-bonding network using WHAT IF (50,51).

ESIs were calculated using the program PIPSA (53,54) and analyzed according to the clustering method described in De Rienzo et al. (54). First, the APBS program (55) with the PARSE parameter set (44) was used to compute the molecular electrostatic potentials of the proteins at ionic strengths corresponding to 0 mM and 150 mM and a temperature of 298 K. A grid dimension of 161 × 161 × 161 $Å^3$ with a 0.8 Å grid spacing was used, centered on the global center of mass of the superimposed structures. The dielectric coefficients of the protein and the solvent were set to 2 and 78.5. The dielectric boundary was determined from the van der Waals surface of the protein, and dielectric boundary smoothing was implemented. Second, pairwise ESIs were calculated on the intersection of the electrostatic potentials of the proteins using the whole grid potentials from the APBS calculation. Third, the comparison of the ESIs was carried out by constructing a distance matrix, which was used to cluster proteins of similar electrostatic potentials by projecting the distance matrix onto the Euclidian space, as described in De Rienzo et al. (54). Clustering of proteins with similar ESIs was visualized and plotted using the program MAGE (56).

Molecular graphics

Molecular graphics have been created with the programs MOLMOL (57), Swiss PDB viewer (26), and GRASP (49,52). Nomenclature compatibility between PDB, WHAT IF, UHBD, MOLMOL, and GRASP and preparation for UHBD runs was attained using a series of homemade PERL scripts.

RESULTS

Previous studies on the interaction of RCAs or CRs with complement components have shown the importance of the overall electrostatic potential and complementary surface charge for recognition and association. These studies involve the characterization of the CR1-C3b (36), CR1-C4b (36,58), CR2-C3d (23,59–61), MCP-C3b/C4b (62), DAF-Factor B (63), and VCP-heparin (17,18,64) interactions, and the function of viral proteins VCP/SPICE (21,22), and Kaposi's sarcoma-associated herpesvirus complement control protein, KCP (also known as Kaposi's sarcoma-associated herpesvirus inhibitor of complement activation, KAPOSICA) (10,65). These studies prompted us to explore the dynamic and electrostatic properties of VCP and SPICE, with the goal to explain their difference in binding to C3b and the measured up to 1000-fold higher complement inhibitory activity for SPICE (21,22). We have also extended our studies to include a two-amino acid mutant of VCP (called VCP2m) with higher complement inhibitory activity than VCP and nearly equal activity as SPICE (21). Based on our modeling for VCP, SPICE, and VCP2m, we predict that a four-amino acid mutant of VCP (called VCP4m) should have higher inhibitory activity than SPICE and that a three-amino acid mutant (called VCP3m) should have lower inhibitory activity than VCP. Fig. 1 shows the sequence alignment of VCP, SPICE, and their two-, three-, and four-amino acid mutated analogs with predicted enhanced or reduced complement inhibitory activities compared to VCP. Fig. 1 also depicts the sequence alignment among the four homologous CCP modules per protein. The rationale for the design of the mutants, based on their electrostatic properties, is described below.

We have performed MD simulations for VCP to eliminate unfavorable crystal packing effects, to reach an energetically global minimum for its structure, and to determine its conformational flexibility and mobility and correlated modular motions. We define here flexibility as the backbone and side-chain dynamics within each CCP module and mobility as the intermodular dynamics. We have also performed MD for SPICE and the three mutants of Fig. 1 to optimize their modeled structures and to examine their structural integrity and dynamics. Fig. 2 shows the initial minimized structure of VCP and final minimized structures of 10 ns MD simulations for VCP, SPICE, VCP2m, VCP3m, and VCP4m. The initial structures are nearly identical for all proteins because they are based on structural homology modeling using the crystal structure of VCP as a template. Simple energy minimization was applied to the initial structures that corrected for local unfavorable interactions introduced by the mutations. Fig. 2, *B–F*, depicts the intermodular mobility of VCP/SPICE and their mutants at 10 ns, whereas the structures of the individual modules are nearly invariable within the definition for the structure of CCP modules (16). According to CATH classification (66) the CCP module belongs in the ''mainly β''-class, ''ribbon'' architecture, and ''complement module'' topology and homologous superfamily. A more complete presentation of the integrity of individual modular structures and the intermodular dynamics during the MD trajectories, with sampling for every nanosecond, can be found in the Supplementary Material.

Fig. 3 shows the RMSD time series for each CCP of VCP, SPICE, VCP2m, VCP3m, and VCP4m. In the 8–10 ns time frame, the backbone RMSDs for every CCP module have reached plateau values of stable state for all proteins, with small RMSD fluctuations depicting the backbone flexibility for individual CCP modules. Given the backbone RMSD's behavior and the objective of our study, it was deemed unnecessary to continue our MD simulations for longer than 10 ns. Our objective was to perform a comparative study of the intramodular flexibilities and intermodular mobilities, at a given time range, for five homologous proteins differing by only 2–11 amino acids, rather than a study of the absolute time evolution of each protein structure. We have used the 10 ns structures to evaluate the titration properties of the proteins

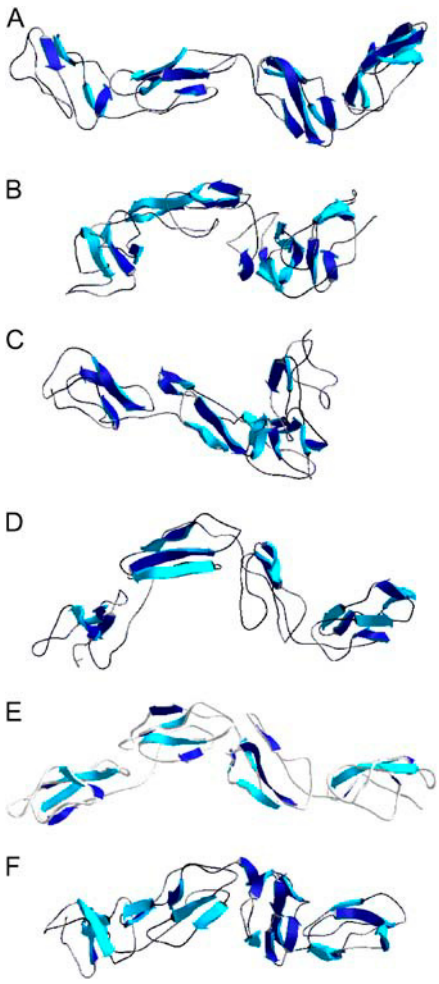

FIGURE 2 Ribbon models for the initial minimized crystal structure of VCP (*A*) and the final (10 ns) structures from the MD simulations of VCP (*B*), SPICE (*C*), VCP2m (*D*), VCP3m (*E*), and VCP4m (*F*).

and the last 2 ns of the MD simulations to quantify the intermodular dynamics or mobility and the spatial distribution of the electrostatic potentials.

Table 1 shows an analysis of intermodular dynamics, using the tilt, skew, and twist angles for modules CCP1-CCP2, CCP2-CCP3, and CCP3-CCP4. The use of tilt, skew, and twist angles is a standard choice in the literature for the evaluation of the intermodular topology of CCP-module-containing receptors, regulators, and inhibitors of the complement system (16,19,20,34–37). Further analysis of intermodular dynamics was performed using solvent accessibilities. The use of solvent accessibilities has been a semiquantitative criterion for the comparison of intermodular contacts across several complement RCAs and CRs (16); however, these studies used static crystallographic structures without taking into account intermodular mobilities. Fig. 4 shows the difference in SASA of the sum of the four individual modules minus the SASA of the whole proteins for VCP, SPICE, VCP2m, VCP3m, and VCP4m. This figure depicts the loss or gain of solvent accessibility by the formation or deformation of intermodular contacts during the MD trajectories. More contacts are formed at 10 ns than at 0 ns (Fig. 4), which is consistent with the molecular graphics of Fig. 2 and Supplementary Material.

Correlated intermodular motions during the MD trajectories were estimated using covariance analysis. Fig. 5 shows the cross correlations of CCP module displacements (indeed oscillations) from their average position during the MD trajectory for VCP, SPICE, VCP2m, VCP3m, and VCP4m. There are differences in the motional behavior of module CCP1 between VCP and SPICE, despite the fact that the sequence of this module is identical in the two proteins (the 11-amino acid differences between VCP and SPICE are located in modules CCP2-3). Specifically, the motion for pairs (CCP1, CCP2) and (CCP1, CCP3) is anticorrelated in VCP and correlated in SPICE (Fig. 5). Opposite motional behavior is observed for pairs (CCP2, CCP4) and (CCP3, CCP4) between VCP and SPICE, whereas pairs (CCP1, CCP4) and (CCP2, CCP3) show similar behavior (Fig. 5). It should be noted that VCP, VCP2m, VCP3m, and VCP4m demonstrate overall similar motional behavior for CCP1 with the exception of the motion of (CCP1, CCP2) in VCP4m which is uncorellated (Fig. 5). The double mutation in CCP2 of VCP2m has a significant effect in the relative motion of the pair (CCP2, CCP3), compared to VCP, and smaller effects on the remaining pairs, mainly in the magnitude of the cross correlations. The added, compared to VCP2m, double mutation in CCP1 of VCP4m has a more profound effect in the relative motions of the pairs (CCP1, CCP2), (CCP2, CCP3), (CCP2, CCP4), and (CCP3, CCP4). Incorporation of two mutations in the loop CCP1-2 and one mutation in the loop CCP3-4 of VCP3m affects mainly the motional behavior of the pair (CCP2, CCP4) and to a lesser extent that of (CCP3, CCP4) compared to VCP (Fig. 5).

Fig. 6, *A* and *B*, shows the spatial distribution of the electrostatic potentials of VCP and SPICE for the energy-minimized initial structures and snapshots from the last 2 ns of the MD trajectories. The figure depicts the fluctuations of the structure and the electrostatic potential at the beginning and during the end of the MD simulation. A more complete set of figures showing the modulation of electrostatic potentials in 1-ns MD snapshots is given in the Supplementary Material. The electrostatic potential of VCP consists of predominantly positive potential at the terminal CCP modules, CCP1 and CCP4, with a protruding patch of negative potential in CCP1 and predominantly negative potential at the CCP2-CCP3 interface (Fig. 6, *A* and *B*). The electrostatic potential of SPICE consists of predominantly positive potential with patches of small negative potential in CCP1, CCP4, and the CCP2-CCP3 interface (Fig. 6, *C* and *D*). Some cancellation between positive and negative potentials occurs at the CCP1-CCP2 and CCP3-CCP4 interfaces (Fig. 6, *C* and *D*). The stronger positive potential of SPICE reflects the E-108K/E-120K (CCP2), E-144N/D-178N (CCP3), and

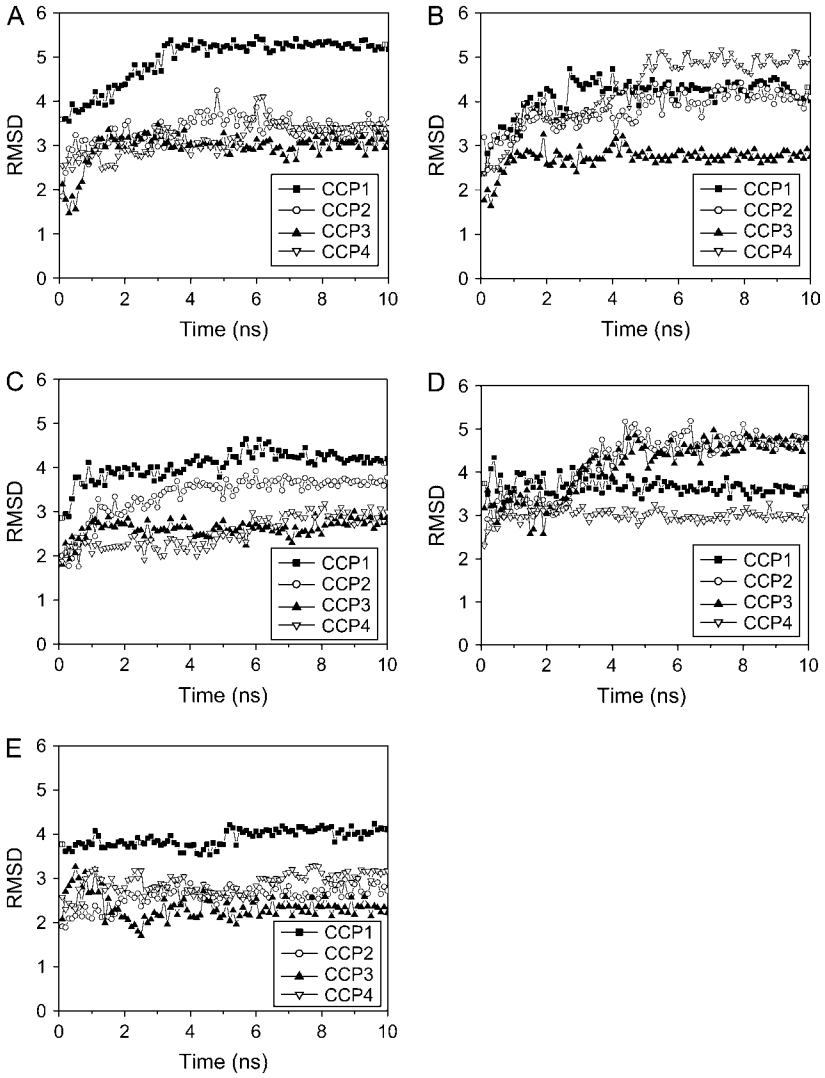

FIGURE 3 Backbone heavy atom RMSDs per CCP module. (*A*) VCP, (*B*) SPICE, (*C*) VCP2m, (*D*) VCP3m, and (*E*) VCP4m. The backbone heavy atoms N, C_α, and C were used to calculate the RMSDs from the minimized crystal structures. The stable structures of the last two nanoseconds were used to calculate intermodular skew, tilt, and twist angles (Table 1) and electrostatic potentials (Fig. 6). The MD structures at 10 ns were used to calculate the predicted titration curves and apparent pK_a values (Figs. 8 and 9).

K-214T/K-236Q (CCP4) mutations compared to VCP. These mutations account for an overall +4 charge difference in favor of SPICE, considering that the Q-77H and H-98Y mutations compensate for each other if the two histidines have the same charge state. The difference in the up to 1000-fold higher activity of SPICE compared to VCP has been attributed to their differences in the strength and topology of their electrostatic potentials (21).

TABLE 1 Intermodular mobility using the tilt, skew, and twist angles for the CCP1-CCP2, CCP2-CCP3, and CCP3-CCP4 modules during the last 2 ns of the MD trajectories

	Tilt angle			Skew angle			Twist angle		
Protein	CCP1–CCP2	CCP2–CCP3	CCP3–CCP4	CCP1–CCP2	CCP2–CCP3	CCP3–CCP4	CCP1–CCP2	CCP2–CCP3	CCP3–CCP4
VCP	89.3–10.2/ +8.0	97.1–20.0/ +15.2	115.7–10.5/ +9.3	100.9–9.8/ +11.7	−138.9–17.4/ +18.5	94.9–15.9/ +17.0	128–27.5/ +25.1	−1.75–21.9/ +23.0	28.4–14.3/ +11.8
SPICE	23.0–7.4/ +9.5	62.3–10.7/ +15.2	111.0–8.2/ +9.8	0.9–23.1/ +23.2	162.1–10.6/ +14.5	79.1–15.1/ +17.5	30.9–12.4/ +16.9	−67.5–13.8/ +22.4	−57.3–15.9/ +21.5
VCP2m	36.9–12.8/ +13.1	91.5–14.9/ +25.0	101.1–17.8/ +16.3	20.0–18.9/ +22.0	−111.1–10.4/ +13.6	124.1–21.2/ +14.3	83.4–31.2/ +17.7	−22.0–18.0/ +18.0	26.3–19.6/ +41.4
VCP3m	10.2–6.2/ +11.3	75.1–13.7/ +12.2	74.4–19.1/ +18.0	−55.8–35.5/ +43.3	−144.8–25.1/ +31.5	19.3–19.2/ +26.5	97.2–24.0/ +33.1	−4.4–25.6/ +21.0	−81.6–33.1/ +35.9
VCP4m	54.3–9.8/ +8.1	116.6–7.9/ +10.4	104.3–20.7/ +17.1	107.2–9.7/ +17.4	141.3–14.0/ +14.6	32.1–27.7/ +24.8	86.6–11.2/ +16.2	−31.7–26.3/ +26.5	−63.9–41.2/ +32.5

The mean angle values are shown with the ranges that provide the minimum and maximum angle values.

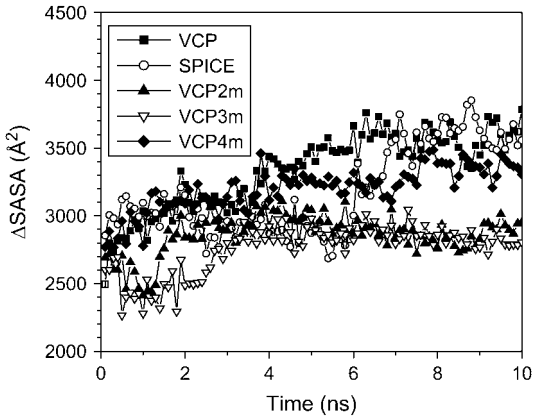

FIGURE 4 Calculated difference in the SASA (ΔSASA) during the MD trajectory. ΔSASA is the SASA of the sum of individual CCPs minus the SASA of the whole protein.

Fig. 6, *E–J*, shows the spatial distribution of the electrostatic potential of VCP2m, VCP3m, and VCP4m for the energy-minimized initial structures and snapshots from the last 2 ns of the MD trajectories. The VCP2m mutant was designed to possess similar spatial distribution of its electrostatic potential as SPICE, with minimum number of mutations using the static x-ray structure of VCP in a previous study (21). VCP2m has two amino acid mutations, E-108K and E-120K, in CCP2 as opposed to 11 amino acid mutations of SPICE in CCP2-4 (Fig. 1). SPICE and VCP2m were shown to be the most active VCP analogs in inhibiting C3b; however, their binding profiles to C3b were distinct as demonstrated by surface plasmon resonance (21), possibly reflecting their dynamic differences (Fig. 6, *C–F*).

Based on the character of the electrostatic potentials of VCP, SPICE, and VCP2m we designed the VCP3m analog with the three-amino acid mutations critically positioned to nearly eliminate the spatial distribution of the positive electrostatic potential in CCP1-3 (Fig. 6, *G* and *H*). The mutations are K-64E, R-66E in the CCP1-2 loop and K-186E in the CCP3-4 loop. The loop locations were chosen for mutations because the inherent internal flexibility and solvent exposure of the loops is unlikely to affect the tertiary structure of the CCP modules. Similarly we designed the VCP4m analog with minimal four-amino acid mutations positioned to enhance the spatial distribution of the positive electrostatic potential in CCP1-3 (Fig. 6, *I* and *J*). VCP4m has the same mutations as VCP2m (E-108K and E-120K in CCP2) with the addition of E-18K and E-32K in CCP1. VCP4m introduces mutations in the first module, which is free of mutations in SPICE. Each mutation in VCP2m, VCP3m, and VCP4m resulted in altering the sign of the charge and a change of ± 2 charge units. The mutated amino acids had percent SASAs of more than 25% in the crystal structure of VCP. A solvent-exposed amino acid can usually be mutated without disturbing the global structure, which is stabilized mainly by hydrophobic interactions of the protein core and disulfide bridges in the case of CCP modules. Locally, solvent exposure allows the mutating amino acid to reorient itself during the MD simulation to form new favorable hydrogen bonds and salt bridges or local networks of electrostatic interactions in general. We predict that VCP3m should demonstrate reduced binding and activity properties and VCP4m should demonstrate enhanced binding and activity properties.

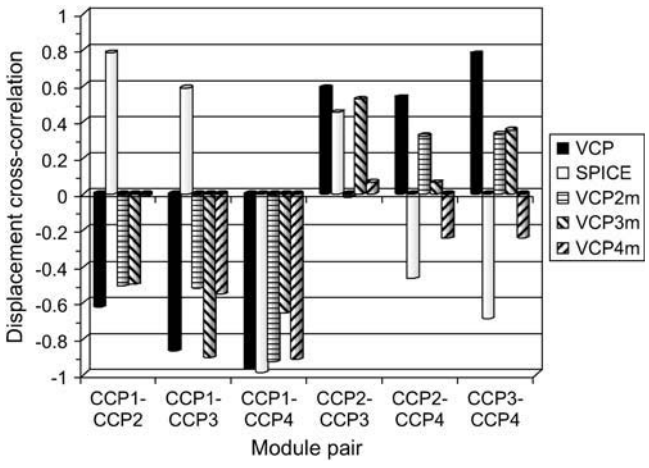

FIGURE 5 Calculated cross correlations of the displacements of pairs of CCP modules for VCP (*black*), SPICE (*white*), VCP2m (*horizontal fill*), VCP3m (*downward diagonal fill*), and VCP4m (*upward diagonal fill*).

The electrostatic potentials in Fig. 6 are calculated using ionic strengths corresponding to 0 mM and 150 mM salt. The isopotential surfaces are plotted at ± 1 k_BT/e in all cases. Comparison of the isopotential surfaces using 0 mM and 150 mM salt provides a quantification of electrostatic screening of the protein electrostatic potentials by the salt ions. Plots at 0 mM salt exaggerate the electrostatic potential profiles, whereas plots at 150 mM salt demonstrate the presence of variable electrostatic screening by the salt ions, depending on the local protein structure and charge. The 150 mM salt concentration was chosen because it resembles the physiological ionic strength in serum. The 0 mM salt concentration was chosen to demonstrate the extreme magnitude of electrostatic interactions (Coulombic and desolvation effects) of the proteins. It also models in vitro experiments performed in the absence of salt.

To quantify the differences of the electrostatic potentials we have calculated ESIs among the five proteins, using the minimized structures. ESIs provide a quantitative measure of the similarity between the magnitudes and distributions of the electrostatic potentials of two proteins. Fig. 7 shows the three-dimensional distributions of the ESIs in the form of similarity distances. In a coarse analysis, the active or predicted active proteins, VCP, SPICE, VCP2m, and VCP4m, are clustered together whereas the predicted inactive VCP3m forms a cluster by itself. In a finer analysis three clusters can be distinguished: SPICE, VCP2m, and VCP4m are clustered together, VCP forms a cluster by itself, and VCP3m forms a

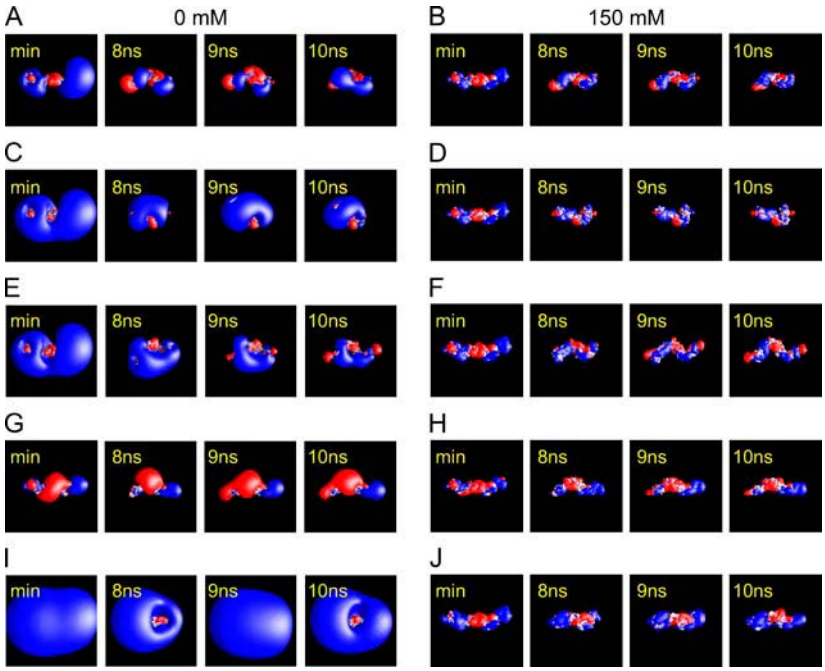

FIGURE 6 Isopotential surfaces at ± 1 k_BT/e, comparing the fluctuations of the spatial distribution of electrostatic potentials for the initial minimized crystal structures and the 8, 9, and 10 ns MD structures. (*A* and *B*) VCP, (*C* and *D*) SPICE, (*E* and *F*) VCP2m, (*G* and *H*) VCP3m, and (*I* and *J*) VCP4m. The electrostatic potentials were calculated using 0 mM salt concentration (*left columns*) and 150 mM salt concentration (*right columns*).

cluster by itself. The choice of the minimized structures for the ESI calculation was made to assure a fair comparison among the five proteins while they are in a similar overall conformation.

We have calculated the apparent pK_a values for each ionizable amino acid of VCP, SPICE, and their mutants using the 10 ns MD structures. Lists of predicted apparent pK_a values are provided in the Supplementary Material. Fig. 8 shows examples of predicted titration curves for H-140 of VCP/SPICE and their mutants, E-108 and E-120 of VCP and K-108 and K-120 of SPICE. H-140 shows lower apparent pK_a value from its model pK_a value of 6.3 in both VCP and SPICE, suggesting somehow unfavorable interactions. However, H-140 shows higher apparent pK_a value in VCP2m, suggesting favorable interactions (Fig. 8 *A* and Supplementary Material). E-108 of VCP has a lower apparent pK_a value than a free glutamic acid in solution, suggesting overall favorable electrostatic environment (Fig. 8 *B* and Supplementary Material). The apparent pK_a value for E-120 of VCP is identical to the pK_a of free glutamic acid in solution. K-108 and K-120 of SPICE have apparent pK_a values close to those of free lysines in solution (Fig. 8 *B* and Supplementary Material).

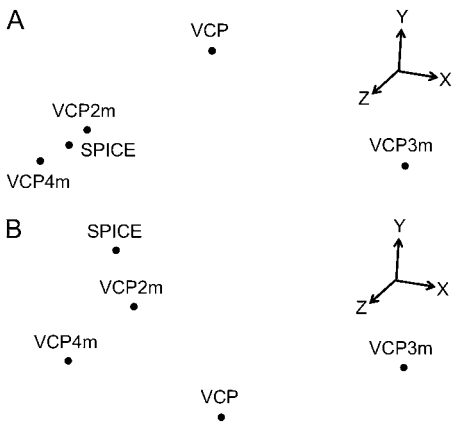

FIGURE 7 Three-dimensional plots of ESI distances for VCP, SPICE, VCP2m, VCP3m, and VCP4m. ESIs were calculated at ionic strengths corresponding to 0 mM (*A*) and 150 mM (*B*) concentrations. The plot shows the distinct clustering of the proteins according to the similarity of their electrostatic potentials.

We hypothesized that the observed subtle binding differences between SPICE and VCP2m (21) may be due to the differences in the apparent pK_a values of H-140 (Fig. 8 *A*). To further examine this hypothesis we have evaluated the titration curves of VCP, SPICE, VCP2m, VCP3m, and VCP4m. Fig. 9 shows the mean net charge changes as a function of pH. Fig. 9 *B* depicts the mean net charge at the vicinity of the physiological pH, with the mean net charge at pH 7 marked in the figure. There is a 1.1 unit charge difference between SPICE (mean net charge 5.9) and VCP2m (mean net charge 7.0) at pH 7. Examination of the calculated apparent pK_a values (Supplementary Material) suggests that this charge difference may arise from the apparent pK_a differences of H-140 in SPICE and VCP2m. This hypothesis implicates H-140, together with the variable modulation of the electrostatic potentials (Fig. 6, *C–F*) and the distinct modular motions (Fig. 5) in explaining the subtle differences in binding to C3b between SPICE and VCP2m. Increase of the positive mean net charge in the order VCP3m $<$ VCP $<$ VCP2m $\sim$ SPICE $<$ VCP4m correlates well with increase in measured activities for VCP, SPICE, and VCP2m (21).

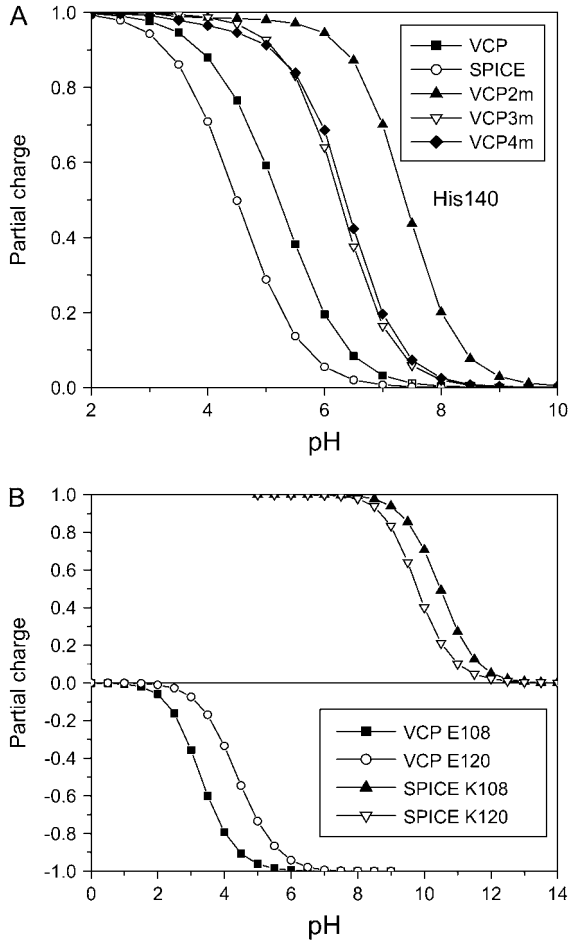

FIGURE 8 Selected titration curves for H-140 of VCP, SPICE, VCP2m, VCP3m, and VCP4m, E-108, E-120 of VCP, and K-108, K-120 of SPICE. The MD structures at 10 ns were used to calculate the predicted titration curves.

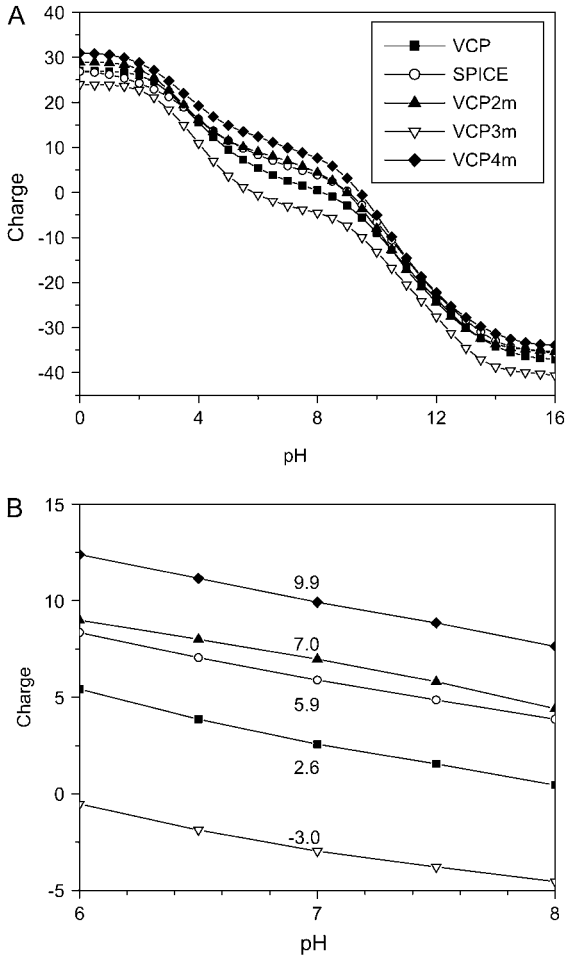

FIGURE 9 pH dependence of mean net charge for VCP, SPICE, VCP2m, VCP3m, and VCP4m. (*A*) pH range 0–16. (*B*) The vicinity of physiological pH in the range of 6–8, with the mean net charge at pH 7 marked. The MD structures at 10 ns were used to calculate the charges.

DISCUSSION

We have performed MD simulations for VCP and a series of VCP analogs with a minimal number of mutations that have or are predicted to have variable abilities against binding to C3b/C4b and inactivation of the complement system. One of these analogs is SPICE a homologous *Orthopoxvirus* protein with higher complement inhibitory activity (21,22). VCP and SPICE have only 11 amino acid differences in their 244 amino acid sequences. The MD simulations aim to shed light on the intermodular mobility, variability of the overall shape, intramodular flexibility, and structural integrity of the modeled proteins during the MD trajectories of each protein but also in comparison with each other. A long-standing question in the field of complement research deals with the linearity, or not, of multi-modular CCP-containing proteins, such as CR1, CR2, Factor H, MCP, DAF, and VCP (16,67,68). CR1 consists of 30 CCP modules, CR2 of 15, Factor H of 20, and MCP, DAF, and VCP of 4 CCP modules. The CCP modules in these proteins form linear chains connected with short flexible loops. There are several structures of individual, pairs, triplets, or quartets of modules for these structures deposited at the PDB (25) from NMR or x-ray diffraction studies (reviewed in Soares and Barlow (16)). VCP is a protein with complete four-modular structure (17) deposited at the PDB and thus a good model system for computational studies. Another question that often arises with CCPs is the relation between their mobility and binding or activity properties. This question could be reformulated as the relation between the spatial distribution of the physicochemical properties of CCPs with binding and activity properties. Earlier studies have shown that the binding and activity of various CCPs is modulated by their electrostatic potentials in the form of long-range interactions (21,23) and/or by their surface charges in the form of short-range electrostatic interactions (23,58–65). We address the relations among dynamics (mobility and flexibility), dynamic spatial arrangement of electrostatic properties, and inhibitory activities for VCP/SPICE and their mutants.

An earlier study has shown a strong correlation between the strength of the positive electrostatic potential of VCP, SPICE, VCP2m, and several other analogs with their binding and activity properties (21). That study used rather simplistic modeling of the electrostatic potentials based on the solution of Coulomb's equation and without the use of partial charges to account for the electric dipoles within the proteins. It also used the rigid and unrelaxed crystallographic structure of VCP for structural homology modeling and for the evaluation of the electrostatic potentials. Here we have used snapshots from MD trajectories to evaluate the electrostatic potentials of VCP, SPICE, and VCP2m, for which we have experimental binding and activity data. We have calculated the electrostatic potentials using the Poisson-Boltzmann equation and have included partial charges for the electric dipoles. The improved calculation reveals a significant difference in the electrostatic character of the CCP4 module of VCP, which is predominantly positive. This was not shown in the previous study (21). We also propose that a new analog with three-amino acid mutations, VCP3m, should demonstrate diminished binding and activity and a new analog with four-amino acid mutations, VCP4m, should demonstrate stronger binding and higher activity. The selection of the mutated amino acids for VCP3m was chosen to significantly reduce the overall positive electrostatic potential of VCP, without a major effect on the structural integrity of the protein. The mutated amino acids are solvent exposed at the intermodular loops of CCP1-2 and CCP3-4 and are expected to affect the intermodular dynamics but not the structure of individual CCP modules. The selection of the mutated amino acids for VCP4m was chosen to significantly enhance the overall positive electrostatic potential of VCP, without significantly disrupting the structure of individual CCP modules. Our selection of mutations is based not only on altering the charge balance but also on altering the spatial distribution of the electrostatic potential, which takes into account cancellation of positive and negative potentials. In addition, we have calculated the apparent pK_a values for all ionizable amino acids of VCP, SPICE, VCP2m, VCP3m, and VCP4m for the final MD structures to generate a database of the amino acids that participate in favorable or unfavorable Coulombic or desolvation electrostatic interactions.

Our MD simulations have explored the flexibility of the individual CCP modules of VCP/SPICE and their mutants (Fig. 2), in the form of the calculated RMSDs (Fig. 3), and the mobility of CCP modules with respect to each other, in the form of differences in SASA (Fig. 4), the tilt, skew, and twist angles (Table 1), and covariance analysis (Fig. 5). We have evaluated structural integrity by examining the secondary structure and tertiary fold of individual CCP modules (Fig. 2 and Supplementary Material). We have used snapshots during the MD trajectories to explore the spatiotemporal distribution of the electrostatic potentials of VCP and SPICE (Fig. 6). We show that the spatial distribution of the electrostatic potentials varies during the MD trajectories with variable degrees of positive-negative cancellation. Overall, the active or predicted active proteins have predominantly positive electrostatic potentials, with increasing strength in the order VCP3m $<$ VCP $<$ VCP2m $\sim$ SPICE $<$ VCP4m. Small patches of negative potential appear and disappear in individual CCP modules during the MD trajectories (Fig. 6 and Supplementary Material). Previously, it was proposed using static structures that the increase of the positive potential in modules CCP1 and CCP4 and decrease of negative potential at the interface of modules CCP2-CCP3 was responsible for increase in binding and activity (21). Here we propose that the overall positive electrostatic potential of VCP, SPICE, VCP2m, and VCP4m is responsible for recognition with a region of negative potential in C3b/C4b through long-range electrostatic interactions, irrespective of the overall shape of the highly dynamic modular proteins. However, we expect that a particular topology will be favored for binding to C3b/C4b through local pairwise electrostatic interactions in the form of hydrogen bonds and salt bridges or networks of multiple electrostatic interactions and nonpolar effects, in addition to long-range electrostatic effects. Our studies are sufficient to predict the association and activity properties of VCP, SPICE, VCP2m and correlate well with measured binding and activity parameters from published experimental data (21). When experimental data for VCP3m and VCP4m become available, we will be able to further refine our hypotheses. We should note that the end result of covering mutated VCP with a positive electrostatic potential (for active) or a negative electrostatic potential (for inactive) can be achieved by a number of different combinations of amino acid mutations. Here we chose the least number of mutations, which were the least destructive for the structures of individual CCP modules.

The use of correlations between electrostatic potentials and the functionality of sets of homologous proteins has been demonstrated before, most notably in the studies by Wade and co-workers (53,54,69,70). The correlations suggest that if two proteins share similar electrostatic potential profiles, they are likely to interact with the same targets. In the case of similar electrostatic potential profiles, variation in the overall strength of the potentials, locally or globally, can be correlated with variable binding and function for electrostatically driven processes. This is the case for the group VCP, SPICE, VCP2m, VCP3m, and VCP4m, as shown in Fig. 7. The calculated ESIs provide an effective means of differentiation between predicted active from predicted inactive proteins in the studied group of VCP/SPICE proteins and their mutants. Specifically, the spatial arrangement of the ESIs demonstrates the presence of three subgroups in the following order of increasing activity: VCP3m $<$ VCP $<$ (VCP2m, SPICE, VCP4m) (Fig. 7). In addition to comparisons across proteins made with ESIs, the cross correlations of modular displacements, discussed below, were useful to quantify correlated motions within the same protein and to make motion-activity comparisons across proteins.

Overall, the effect of mutations in the correlated oscillatory motions of pairs of CCP modules is variable. The anticorrelation of the motion of modules (CCP1, CCP4) (Fig. 5) can be explained by the repulsive Coulombic interaction of the overall positive potential of modules CCP1 and CCP4 in all proteins (Fig. 6). The smaller anticorrelation for module pair (CCP1, CCP4) of VCP3m (Fig. 5) may be due to a more balanced potential in CCP1 compared to the rest of the proteins (Fig. 6). The magnitude of the anticorrelated motion of the module pair (CCP1, CCP4) differentiates, to a certain extent, the predicted active proteins, VCP, SPICE, VCP2m, and VCP4m (cross correlation of -0.91 to -0.99) from the predicted inactive protein, VCP3m (cross correlation of -0.66; Fig. 5). Similar direct arguments for potential/motion correlation cannot be made when the middle modules are involved because of more complex interactions, more balanced charge, and dynamic canceling of positive and negative electrostatic potentials depending on their spatial distribution. Overall, SPICE demonstrates very distinct behavior compared to VCP, VCP2m, VCP3m, and VCP4m, reflecting the combined effect of the 11 mutations in the intermodular dynamics. A more detailed principal component analysis using individual (x, y, z) coordinate displacements, as opposed to the vector, r(x, y, z), for modules and for C_α-atoms will be the subject of future analysis.

Based on our pK_a calculations and the titration curves of the proteins, we propose that the subtle differences in binding of SPICE and VCP2m to C3b (21) may be attributed to differences in the protonation state of H-140 (Figs. 8 and 9). The local environment of H-140 is influenced by differences in the intermodular mobility of SPICE and VCP2m (Fig. 6). Our study is an example of the use of electrostatic potentials to predict activities for VCP/SPICE and their mutants.

In essence, our studies suggest a two-step model for the interaction of VCP/SPICE and their mutants with their target complement proteins C3b/C4b. The two steps are recognition (formation of an encounter complex) and binding (formation of the final complex). The global electrostatic potentials model the recognition step. Detail modeling of the binding step is not possible at the time because of the absence of structural information of the formed complexes and their binding sites. Our two-step model is in the same line of thought as our earlier study for CR2-C3d association (23). In the CR2-C3d study we were able to be more specific on the mechanism of association because we had available and used the three-dimensional structures of free CR2 (71), free C3d (61), and CR2-C3d complex (60), where CR2 contained only the first two CCP modules, which are responsible for association with C3d. The first step involved recognition through long-range electrostatic interactions; and the second step involved the actual binding through electrostatic interactions (long-range and short-range in the form of hydrogen bonds, salt bridges, and desolvation), hydrophobic, and van der Waals interactions, in addition to entropic effects involving the solvent exclusion and local structural rearrangements at the binding sites (23). Based on the electrostatic potentials of a predominantly positively charged CR2 and a predominantly negatively charged C3d, we were able to explain the binding abilities for C3d mutants at and away from the association interface (23). A subsequent experimental study has produced additional mutational analysis on the CR2 component of the CR2-C3d complex with the overall findings in agreement with CR2-C3d association driven by electrostatics, although the authors focus their analysis on short-range effects (59).

Some of our theoretical predictions for the involvement of individual amino acids in function have been previously addressed by experimental studies. According to our model, the recognition step depends on long-range electrostatic properties. The kinetic and binding variations observed for a number of VCP mutants in a previous study using surface plasmon resonance (21) are due to combined long- and short-range interactions. Several of our mutated VCP acidic amino acids to basic in VCP2m and VCP4m are indeed basic amino acids in the homologous CCP modules of CR1 (the C3b/C4b binding Site 2, modules CCP8–10 and CCP15–17) (16). Also, homologous amino acids in MCP have variable charge. Specifically, the VCP mutations (homologous residues for CR1, MCP, respectively, in parentheses) are E-18K (K-912, E-11), E-32K (K-929, D-27), K-64E (K-959, R-62), R-66E (K-961, -), E-108K (I-1005, E-108), E-120K (K-1016, K-119), K-186E (K-1095, K-193). Structure-guided mutagenesis studies of the C3b/C4b binding site 2 of CR1 (modules CCP15–17 for which there are structures) have shown that the corresponding basic amino acids for VCP positions 18, 64, 66, and 120 (K-912, K-959, K-961, and K-1016) when mutated to neutral or negative amino acids (in single or multiple mutations) resulted to reduction or abrogation of activity (discussed collectively with other similar mutations in Smith et al. (36) and Krych-Goldberg et al. (72)). The authors of these studies treat the mutations of basic to neutral or acidic amino acids in view of mainly local interactions; however, in some instances they were able to separate global (or nonspecific according to Krych-Goldberg et al. (72)) from local electrostatic effects. Mutations of charged amino acids in the CCP2–4 modules of MCP, including corresponding VCP positions 120 and 186 (K-119 and K-193 in MCP), also demonstrate influence in C3b/C4b binding and/or cofactor activity for C3b and C4b degradation (62). Also, based on mutation of one tyrosine of the Y-97, Y-98 pair in MCP, it has been previously discussed that these tyrosines may be important for C4b cofactor activity (22,62). SPICE has a similar pair of tyrosines, from which Y-97 demonstrates unusually high pK_a value (Supplementary Material) due to local electrostatic interactions. Our predicted apparent pK_a values (Supplementary Material) depict a number of ionizable amino acids that participate in networks of electrostatic interactions but have not been previously discussed in the literature. Overall, our study combines a

macroscopic approach for the effect of the electrostatic potentials in recognition and an amino acid-specific approach, in the form of pK_a values, for global or local association effects.

Our data suggest that intermodular dynamics are an integral part of the function of VCP/SPICE and their mutants. Mutations not only at intermodular loops but also at individual CCPs result in differences in intermodular dynamics (Figs. 2, 4, 5, and 6, and Supplementary Material). For our detailed analysis of intermodular dynamics, we have used the last 2 ns of the MD trajectories, during which the RMSDs per module have reached stable states (Fig. 3). The variability of the intermodular angles (Table 1) suggests that an exact intermodular topology may not be necessary for recognition and that the binding sites may be dynamic in nature. Variability of intermodular angles has been observed before in comparative studies of x-ray and NMR structures of RCAs and CRs made of CCPs (16,35).

NMR structural and relaxation data have addressed the intermodular mobility in the central region of VCP, modules CCP2-3 (19), and the C-terminal half of VCP, modules CCP3-4 (20). NOE data and the determined time-averaged structures based on simulated annealing and NMR restraints have shown that modules CCP3 and CCP4 share an extensive interface, whereas modules CCP2 and CCP3 do not (19,20). However, it should be noted that the two central CCP modules differ significantly in the NMR structure of VCP(CCP2-3) (19) and the crystal structure of VCP(CCP1-4) (17) and that the crystal structure is not compatible with the observed NOE data (19). These differences may be due to the shorter length of VCP(CCP2-3), crystal packing effects, or sample conditions. In addition, ^{15}N relaxation NMR data for the central CCP2-3 modules were consistent with a large number of intermodular orientations and the presence of interconversion among them (19). The NMR relaxation data also suggest that many of the intermodular orientations are kinked. Other studies of VCP(CCP2-3) have suggested that CCP2-CCP3 are in an elongated arrangement without sharing an extensive intermodular interface, which would have been promoted by kinking (73). This proposal was made using analytical ultracentrifugation measurements and unfolding studies monitored by NMR, differential scanning calorimetry, circular dichroism, and intrinsic tryptophan fluorescence. Care should be taken when comparing data from different biophysical methods collected using different sample conditions, such as concentration, pH, ionic strength, buffer composition, temperature, etc. In the case of VCP(CCP2-3) the differences in the CCP2-3 average orientation between the NMR relaxation and ultracentrifugation data were previously attributed to differences in temperature (19). Overall, our conclusions on intermodular mobility of VCP, based on the MD data, are in agreement with the NMR relaxation data.

Another type of ''mobility'' of the binding surfaces has been proposed earlier within individual CCP modules of CR1 and MCP using NMR relaxation data (74). This study suggested mobile β-strands (and surfaces) in CCPs, which is addressed within the definition of flexibility in our study. Our observation of dynamic binding properties involving mobile CCP modules is an extension of the previous findings in O'Leary et al. (74).

Our data contribute to our understanding of the basic immunophysical properties for CCP modules in VCP and SPICE. The immunophysical properties are the intramodular and intermodular dynamics and the type and spatial distribution of the electrostatic potentials, which are modulated by the intermodular dynamics. Our data also demonstrate the power of dynamic and electrostatic modeling to design VCP/SPICE analogs with higher or lower activities, which can be used as the basis to design agonists or antagonists of the native viral proteins. Also, this type of modeling is useful to design inhibitors of unregulated complement activation in pathological situations, such as autoimmune diseases, ischemia reperfusion injury, trauma, cardiopulmonary bypass surgery, and others.

SUPPLEMENTARY MATERIAL

An online supplement to this article can be found by visiting BJ Online at http://www.biophysj.org.

We thank Dr. Buddhadeb Mallik for valuable discussions and an anonymous reviewer for useful comments regarding the electrostatic potential analysis. We also thank Dr. Thomas Girke and the Bioinformatics Core facility of the University of California, Riverside, Institute for Integrative Genome Biology for the use of computational resources.

This work was partially supported by National Science Foundation grant CTS-0427103 and National Institutes of Health grant R24-GM069736.

REFERENCES

1. Volanakis, J. E., and M. M. Frank, editors. 1998. The Human Complement System in Health and Disease. Marcel-Dekker, New York.
2. Morikis, D., and J. D. Lambris, editors. 2005. Structural Biology of the Complement System. Taylor & Francis/CRC Press, Boca Raton, FL.
3. Walport, M. J. 2001. Advances in immunology: complement (first of two parts). *N. Engl. J. Med.* 344:1058–1066.
4. Walport, M. J. 2001. Advances in immunology: complement (second of two parts). *N. Engl. J. Med.* 344:1140–1144.
5. Carroll, M. C. 2004. The complement system in regulation of adaptive immunity. *Nat. Immunol.* 5:981–986.
6. Cooper, N. R. 1998. Complement and viruses. *In* The Human Complement System in Health and Disease. J. E. Volanakis and M. M. Frank, editors. Marcel-Dekker, New York. 393–407.
7. Rosengard, A. M., and J. M. Ahearn. 1999. Viral complement regulatory proteins. *Immunopharmacology.* 42:99–106.
8. Bernet, J., J. Mullick, A. K. Singh, and A. Sahu. 2003. Viral mimicry of the complement system. *J. Biosci.* 28:249–264.
9. Kotwal, G. J. 2000. Poxviral mimicry of complement and chemokine system components: what's the end game? *Immunol. Today.* 21:242–248.
10. Mullick, J., A. Kadam, and A. Sahu. 2003. Herpes and pox viral complement control proteins: 'the mask of self'. *Trends Immunol.* 24: 500–507.
11. Dunlop, L. R., K. A. Oehlberg, J. J. Reid, D. Avci, and A. M. Rosengard. 2003. Variola virus immune evasion proteins. *Microbes Infect.* 5:1049–1056.

12. Seet, B. T., J. B. Johnston, C. R. Brunetti, J. W. Barrett, H. Everett, C. Cameron, J. Sypula, S. H. Nazarian, A. Lucas, and G. Mcfadden. 2003. Poxviruses and immune evasion. *Annu. Rev. Immunol.* 21:377–423.

13. Mcfadden, G. 2004. Smallpox: an ancient disease enters the modern era of virogenomics. *Proc. Natl. Acad. Sci. USA.* 101:14994–14995.

14. Harrison, S. C., B. Alberts, E. Ehrenfeld, L. Enquist, H. Fineberg, S. L. Mcknight, B. Moss, M. O'Donnell, H. Ploegh, S. L. Schmid, K. P. Walter, and J. Theriot. 2004. Discovery of antivirals against smallpox. *Proc. Natl. Acad. Sci. USA.* 101:11178–11192.

15. Morikis, D., and J. D. Lambris. 2005. The building blocks of the complement system. *In* Structural Biology of the Complement System. D. Morikis and J. D. Lambris, editors. Taylor & Francis/CRC Press, Boca Raton, FL. 1–18.

16. Soares, D. C., and D. J. Barlow. 2005. Complement control protein modules in the regulators of complement activation. *In* Structural Biology of the Complement System. D. Morikis and J. D. Lambris, editors. Taylor & Francis/CRC Press, Boca Raton, FL. 19–62.

17. Murthy, K. H. M., S. A. Smith, V. K. Ganesh, K. W. Judge, N. Mullin, P. N. Barlow, C. M. Ogata, and G. J. Kotwal. 2001. Crystal structure of a complement control protein that regulates both pathways of complement activation and binds heparan sulfate proteoglycans. *Cell.* 104:301–311.

18. Ganesh, V. K., S. A. Smith, G. J. Kotwal, and K. H. M. Murthy. 2004. Structure of vaccinia complement protein in complex with heparin and potential implications for complement regulation. *Proc. Natl. Acad. Sci. USA.* 101:8924–8929.

19. Henderson, C. E., K. Bromek, N. P. Mullin, B. O. Smith, D. Uhrin, and P. N. Barlow. 2001. Solution structure and dynamics of the central CCP module pair of a poxvirus complement control protein. *J. Mol. Biol.* 307:323–339.

20. Wiles, A. P., G. Shaw, J. Bright, A. Perczel, I. D. Campbell, and P. N. Barlow. 1997. NMR studies of a viral protein that mimics the regulators of complement activation. *J. Mol. Biol.* 272:253–265.

21. Sfyroera, G., M. Katragadda, D. Morikis, S. N. Isaacs, and J. D. Lambris. 2005. Electrostatic modeling predicts the activities of orthopoxvirus complement control proteins. *J. Immunol.* 174:2143–2151.

22. Rosengard, A. M., Y. Liu, Z. P. Nie, and R. Jimenez. 2002. Variola virus immune evasion design: expression of a highly efficient inhibitor of human complement. *Proc. Natl. Acad. Sci. USA.* 99:8808–8813.

23. Morikis, D., and J. D. Lambris. 2004. The electrostatic nature of C3d-complement receptor 2 association. *J. Immunol.* 172:7537–7547.

24. Morikis, D., and J. D. Lambris. 2004. Physical methods for structure, dynamics and binding in immunological research. *Trends Immunol.* 25:700–707.

25. Berman, H. M., J. Westbrook, Z. Feng, G. Gilliland, T. N. Bhat, H. Weissig, I. N. Shindyalov, and P. E. Bourne. 2000. The protein data bank. *Nucleic Acids Res.* 28:235–242.

26. Guex, N., and M. C. Peitsch. 1997. SWISS-MODEL and the Swiss-PdbViewer: an environment for comparative protein modeling. *Electrophoresis.* 18:2714–2723.

27. Brooks, B. R., R. E. Bruccoleri, B. D. Olafson, D. J. States, S. Swaminathan, and M. Karplus. 1983. CHARMM—a program for macromolecular energy, minimization, and dynamics calculations. *J. Comput. Chem.* 4:187–217.

28. Lazaridis, T., and M. Karplus. 1999. Effective energy function for proteins in solution. *Proteins.* 35:133–152.

29. Lazaridis, T., and M. Karplus. 1999. Discrimination of the native from misfolded protein models with an energy function including implicit solvation. *J. Mol. Biol.* 288:477–487.

30. Lazaridis, T., and M. Karplus. 2000. Effective energy functions for protein structure prediction. *Curr. Opin. Struct. Biol.* 10:139–145.

31. Ryckaert, J. P., G. Ciccotti, and H. J. C. Berendsen. 1977. Numerical integration of Cartesian equations of motion of a system with constraints: molecular dynamics of N-alkanes. *J. Comput. Phys.* 23:327–341.

32. Nose, S. 1984. A unified formulation of the constant temperature molecular dynamics methods. *J. Chem. Phys.* 81:511–519.

33. Hoover, W. G. 1985. Canonical dynamics—equilibrium phase-space distributions. *Phys. Rev. A.* 31:1695–1697.

34. Bork, P., A. K. Downing, B. Kieffer, and I. D. Campbell. 1996. Structure and distribution of modules in extracellular proteins. *Q. Rev. Biophys.* 29:119–167.

35. Lehtinen, M. J., S. Meri, and T. S. Jokiranta. 2004. Interdomain contact regions and angles between adjacent short consensus repeat domains. *J. Mol. Biol.* 344:1385–1396.

36. Smith, B. O., R. L. Mallin, M. Krych-Goldberg, X. F. Wang, R. E. Hauhart, K. Bromek, D. Uhrin, J. P. Atkinson, and P. N. Barlow. 2002. Structure of the C3b binding site of CR1 (CD35), the immune adherence receptor. *Cell.* 108:769–780.

37. Barlow, P. N., A. Steinkasserer, D. G. Norman, B. Kieffer, A. P. Wiles, R. B. Sim, and I. D. Campbell. 1993. Solution structure of a pair of complement modules by nuclear-magnetic-resonance. *J. Mol. Biol.* 232: 268–284.

38. Ichiye, T., and M. Karplus. 1991. Collective motions in proteins—a covariance analysis of atomic fluctuations in molecular dynamics and normal mode simulations. *Proteins.* 11:205–217.

39. Amadei, A., A. B. M. Linssen, and H. J. C. Berendsen. 1993. Essential dynamics of proteins. *Proteins.* 17:412–425.

40. Antosiewicz, J., J. A. Mccammon, and M. K. Gilson. 1994. Prediction of pH-dependent properties of proteins. *J. Mol. Biol.* 238:415–436.

41. Antosiewicz, J., J. A. Mccammon, and M. K. Gilson. 1996. The determinants of pK_as in proteins. *Biochemistry.* 35:7819–7833.

42. Madura, J. D., J. M. Briggs, R. C. Wade, M. E. Davis, B. A. Luty, A. Ilin, J. Antosiewicz, M. K. Gilson, B. Bagheri, L. R. Scott, and J. A. Mccammon. 1995. Electrostatics and diffusion of molecules in solution—simulations with the University of Houston Brownian dynamics program. *Comput. Phys. Commun.* 91:57–95.

43. Gilson, M. K. 1993. Multiple-site titration and molecular modeling: two rapid methods for computing energies and forces for ionizable groups in proteins. *Proteins.* 15:266–282.

44. Sitkoff, D., N. Bental, and B. Honig. 1996. Calculation of alkane to water solvation free energies using continuum solvent models. *J. Phys. Chem.* 100:2744–2752.

45. Davis, M. E., and J. A. Mccammon. 1990. Electrostatics in biomolecular structure and dynamics. *Chem. Rev.* 90:509–521.

46. Gilson, M. K., M. E. Davis, B. A. Luty, and J. A. Mccammon. 1993. Computation of electrostatic forces on solvated molecules using the Poisson-Boltzmann equation. *J. Phys. Chem.* 97:3591–3600.

47. Gilson, M. K., and B. Honig. 1988. Calculation of the total electrostatic energy of a macromolecular system: solvation energies, binding energies, and conformational analysis. *Proteins.* 4:7–18.

48. Gilson, M. K., and B. H. Honig. 1988. Energetics of charge-charge interactions in proteins. *Proteins.* 3:32–52.

49. Honig, B., and A. Nicholls. 1995. Classical electrostatics in biology and chemistry. *Science.* 268:1144–1149.

50. Nielsen, J. E., K. V. Andersen, B. Honig, R. W. W. Hooft, G. Klebe, G. Vriend, and R. C. Wade. 1999. Improving macromolecular electrostatics calculations. *Protein Eng.* 12:657–662.

51. Vriend, G. 1990. WHAT IF—a molecular modeling and drug design program. *J. Mol. Graph.* 8:52–56.

52. Nicholls, A., K. A. Sharp, and B. Honig. 1991. Protein folding and association—insights from the interfacial and thermodynamic properties of hydrocarbons. *Proteins.* 11:281–296.

53. Blomberg, N., R. R. Gabdoulline, M. Nilges, and R. C. Wade. 1999. Classification of protein sequences by homology modeling and quantitative analysis of electrostatic similarity. *Proteins.* 37:379–387.

54. De Rienzo, F., R. R. Gabdoulline, M. C. Menziani, and R. C. Wade. 2000. Blue copper proteins: a comparative analysis of their molecular interaction properties. *Protein Sci.* 9:1439–1454.

55. Baker, N. A., D. Sept, S. Joseph, M. J. Holst, and J. A. Mccammon. 2001. Electrostatics of nanosystems: application to microtubules and the ribosome. *Proc. Natl. Acad. Sci. USA.* 98:10037–10041.

56. Richardson, D. C., and J. S. Richardson. 1992. The kinemage: a tool for scientific communication. *Protein Sci.* 1:3–9.

57. Koradi, R., M. Billeter, and K. Wuthrich. 1996. MOLMOL: a program for display and analysis of macromolecular structures. *J. Mol. Graph.* 14:51–55.

58. van den Elsen, J. M. H., A. Martin, V. Wong, L. Clemenza, D. R. Rose, and D. E. Isenman. 2002. X-ray crystal structure of the C4d fragment of human complement component C4. *J. Mol. Biol.* 322: 1103–1115.

59. Hannan, J. P., K. A. Young, J. M. Guthridge, R. Asokan, G. Szakonyi, X. J. S. Chen, and V. M. Holers. 2005. Mutational analysis of the complement receptor type 2 (CR2/CD21)-C3d interaction reveals a putative charged CCP1 binding site for C3d. *J. Mol. Biol.* 346: 845–858.

60. Szakonyi, G., J. M. Guthridge, D. W. Li, K. Young, V. M. Holers, and X. J. S. Chen. 2001. Structure of complement receptor 2 in complex with its C3d ligand. *Science.* 292:1725–1728.

61. Nagar, B., R. G. Jones, R. J. Diefenbach, D. E. Isenman, and J. M. Rini. 1998. X-ray crystal structure of C3d: a C3 fragment and ligand for complement receptor 2. *Science.* 280:1277–1281.

62. Liszewski, M. K., M. Leung, W. Y. Cui, V. B. Subramanian, J. Parkinson, P. N. Barlow, M. Manchester, and J. P. Atkinson. 2000. Dissecting sites important for complement regulatory activity in membrane cofactor protein (MCP; CD46). *J. Biol. Chem.* 275: 37692–37701.

63. Lukacik, P., P. Roversi, J. White, D. Esser, G. P. Smith, J. Billington, P. A. Williams, P. M. Rudd, M. R. Wormald, D. J. Harvey, M. D. M. Crispin, C. M. Radcliffe, R. A. Dwek, D. J. Evans, B. P. Morgan, R. A. G. Smith, and S. M. Lea. 2004. Complement regulation at the molecular level: the structure of decay-accelerating factor. *Proc. Natl. Acad. Sci. USA.* 101:1279–1284.

64. Smith, S. A., N. P. Mullin, J. Parkinson, S. N. Shchelkunov, A. V. Totmenin, V. N. Loparev, R. Srisatjaluk, D. N. Reynolds, K. L. Keeling, D. E. Justus, P. N. Barlow, and G. J. Kotwal. 2000. Conserved surface-exposed K/R-X-K/R motifs and net positive charge on poxvirus complement control proteins serve as putative heparin binding sites and contribute to inhibition of molecular interactions with human endothelial cells: a novel mechanism for evasion of host defense. *J. Virol.* 74:5659–5666.

65. Mark, L., W. H. Lee, O. B. Spiller, D. Proctor, D. J. Blackbourn, B. O. Villoutreix, and A. M. Blom. 2004. The Kaposi's sarcoma-associated herpesvirus complement control protein mimics human molecular mechanisms for inhibition of the complement system. *J. Biol. Chem.* 279:45093–45101.

66. Orengo, C. A., A. D. Michie, S. Jones, D. T. Jones, M. B. Swindells, and J. M. Thornton. 1997. CATH—a hierarchic classification of protein domain structures. *Structure.* 5:1093–1108.

67. Perkins, S. J., and P. B. Furtado. 2005. Complement and immunoglobulin protein structures by x-ray and neutron solution scattering and analytical ultracentrifugation. *In* Structural Biology of the Complement System. D. Morikis and J. D. Lambris, editors. Taylor & Francis/CRC Press, Boca Raton, FL. 293–315.

68. Gilbert, H. E., J. T. Eaton, J. P. Hannan, V. M. Holers, and S. J. Perkins. 2005. Solution structure of the complex between CR2 CCP 1–2 and C3d of human complement: an x-ray scattering and sedimentation modelling study. *J. Mol. Biol.* 346:859–873.

69. Schleinkofer, K., U. Wiedemann, L. Otte, T. Wang, G. Krause, H. Oschkinat, and R. C. Wade. 2004. Comparative structural and energetic analysis of WW domain-peptide interactions. *J. Mol. Biol.* 344:865–881.

70. Winn, P. J., T. L. Religa, J. N. D. Battey, A. Banerjee, and R. C. Wade. 2004. Determinants of functionality in the ubiquitin conjugating enzyme family. *Structure.* 12:1563–1574.

71. Prota, A. E., D. R. Sage, T. Stehle, and J. D. Fingeroth. 2002. The crystal structure of human CD21: implications for Epstein-Barr virus and C3d binding. *Proc. Natl. Acad. Sci. USA.* 99:10641–10646.

72. Krych-Goldberg, M., P. N. Barlow, R. L. Mallin, and J. P. Atkinson. 2005. C3b/C4b binding site of complement receptor type 1 (CR1, CD35). *In* Structural Biology of the Complement System. D. Morikis and J. D. Lambris, editors. Taylor & Francis/CRC Press, Boca Raton, FL. 179–212.

73. Kirkitadze, M. D., C. Henderson, N. C. Price, S. M. Kelly, N. P. Mullin, J. Parkinson, D. T. F. Dryden, and P. N. Barlow. 1999. Central modules of the vaccinia virus complement control protein are not in extensive contact. *Biochem. J.* 344:167–175.

74. O'Leary, J. M., K. Bromek, G. M. Black, S. Uhrinova, C. Schmitz, X. F. Wang, M. Krych, J. P. Atkinson, D. Uhrin, and P. N. Barlow. 2004. Backbone dynamics of complement control protein (CCP) modules reveals mobility in binding surfaces. *Protein Sci.* 13:1238–1250.